Inorganic Chemistry

Article

pubs.acs.org/IC

# 1,8-Naphthyridine-Derived $Ni^{2+}/Cu^{2+}$-Selective Fluorescent Chemosensor with Different Charge Transfer Processses

Zhanxian Li,*[,†] Wanying Zhao,[†] Xiaoya Li,[†] Yanyan Zhu,[†] Chunmei Liu,[†] Lina Wang,[†] Mingming Yu,*[,†] Liuhe Wei,[†] Mingsheng Tang,[†] and Hongyan Zhang*[,‡]

[†]College of Chemistry and Molecular Engineering, Zhengzhou University, Zhengzhou 450001, China

[‡]Key Laboratory of Photochemical Conversion and Optoelectronic Materials, Technical Institute of Physics and Chemistry, Chinese Academy of Sciences, Beijing 100190, China

Supporting Information

**ABSTRACT:** A highly fluorescent chemosensor based on 1,8-naphthyridine with high sensitivity and selectivity toward $Ni^{2+}/Cu^{2+}$ over other cations both in aqueous solution over a wide pH range (4−10) and in cellular environments was developed. Counteranions such as acetate, sulfate, nitrate, and perchlorate have no influence on the detection of such metal ions. Ethylenediamine showed high selectivity toward the in situ-prepared $Cu^{2+}$ complex over the $Ni^{2+}$ complex, which can be applied to distinguish $Ni^{2+}$ and $Cu^{2+}$. The $Ni^{2+}$-induced fluorescence on−off mechanism was revealed to be mediated by intramolecular charge transfer from the metal to the ligand, while that by $Cu^{2+}$ involves intramolecular charge transfer from the ligand to the metal, as confirmed by picosecond time-resolved fluorescence spectroscopy and time-dependent density functional theory calculations.

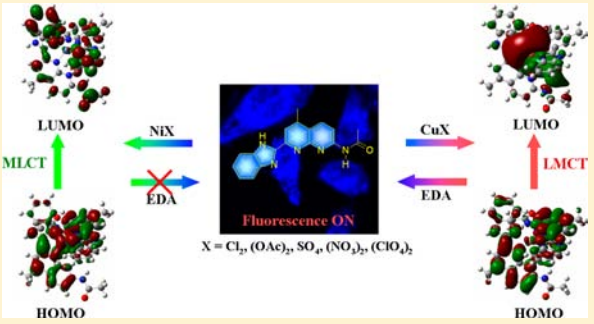


## INTRODUCTION

Fluorescent chemosensors have several advantages over other methods due to their sensitivity, specificity, and ability to be used in real-time monitoring with fast response.[1] Therefore, research on metal-ion-selective fluorescent chemosensors has attracted great attention from chemical scientists, and great achievements have been obtained.[2] $Ni^{2+}$ is a significant environmental pollutant yet an essential trace element in biological systems. For example, loss of nickel homeostasis is harmful to prokaryotic and eukaryotic organisms alike.[3] Nevertheless, reports of $Ni^{2+}$ fluorescent probes are very rare.[4] Copper also plays an important role in various biological processes and is also a significant metal pollutant because of its widespread use.[5] For instance, exposure to a high level of copper even for a short period of time can cause gastrointestinal disturbance, and long-time exposure can cause liver or kidney damage.[6] Many fluorescent $Cu^{2+}$ chemosensors have been reported and used with some success in biological applications.[7] However, some of them have shortcomings for practical applications, such as a low fluorescence quantum yield, low water solubility, and a narrow pH range. Therefore, it is quite essential to design and synthesize $Ni^{2+}/Cu^{2+}$-selective fluorescent chemosensors that have high fluorescence quantum yields, excellent water solubility, and a wide pH range. To develop a novel efficient chemosensor, it is necessary to understand the sensing mechanism. It is well-known that fluorescence is a property of electronically excited states and that the lifetime of the fluorescence decay is a key factor for the mechanism. Therefore, metal ion identification mechanisms can be better explained by fluorescence decay processes as well as quantum-chemical calculations. It is a pity that $Ni^{2+}$ sensing mechanisms have never been reported and that there is only one example about sensing mechanisms of $Cu^{2+}$ with the above two methods.[8]

In this work, we synthesized a new 1,8-naphthyridine-derived compound, 7-acetamidyl-4-methyl-2-(1*H*-benzo[*d*]imidazolyl)-1,8-naphthyridine (**A**), which is highly fluorescent and responsive to $Ni^{2+}$ and $Cu^{2+}$ with excellent selectivity in the presence of excess amounts of various competing metal ions. We found that addition of ethylenediamine (EDA) causes a fluorescence revival of **A** only in the case of $Cu^{2+}$, providing an effective method for distinguishing between $Ni^{2+}$ and $Cu^{2+}$. The fluorescence quenching mechanism was studied by picosecond time-resolved fluorescence (TRF) spectroscopy and density functional theory (DFT) calculations. The application of **A** to the detection of intracellular $Ni^{2+}$ and $Cu^{2+}$ was also achieved.

## EXPERIMENTAL SECTION

**Methods and Materials.** All of the chemicals were purchased from commercial suppliers and used without further purification. All of the reactions were performed under an argon atmosphere using solvents purified by standard methods. $^1H$ and $^{13}C$ NMR spectra were recorded on a Bruker 400 NMR spectrometer. Chemical shifts are reported in parts per million using tetramethylsilane (TMS) as the

**Received:** August 23, 2012
**Published:** October 30, 2012

internal standard. Mass spectra were obtained on a Micromass GCT-MS mass spectrometer.

**Absorption and Fluorescence Spectroscopy.** All spectral characterizations were carried out in HPLC-grade solvents at 20 °C within a 10 mm quartz cell. UV−vis absorption spectra were measured with a TU-1901 double-beam UV−vis spectrophotometer, and fluorescence spectra were determined on a Hitachi F-4500 spectrometer. The fluorescence quantum yield ($\Phi_{fl}$) was measured at room temperature with excitation at 350 nm (Xe lamp in the F-4500 spectrometer) using quinine bisulfate in 1 M $H_2SO_4$ ($\Phi_{fl}$ = 0.546) as the reference.[9]

**Time-Resolved Fluorescence Spectroscopy.** TRF spectra were measured on a LifeSpec picosecond TRF spectrometer (Edinburgh Instruments Ltd.). The sample concentration was set to $1.25 \times 10^{-5}$ M.

**DFT Calculations.** The charge distributions of compounds **A**, **B**, and **C** were calculated with the 6-31G** basis set using the natural bond orbital (NBO) model. DFT calculations using the Becke three-parameter exchange/Lee−Yang−Parr correlation hybrid functional (B3LYP) with 6-31G(d) and 6-31G**+LanLZDZ basis sets as implemented in the Gaussian 09 suite of programs were carried out for the geometry optimizations of **A**, **A**−$Cu^{2+}$ and **A**−$Ni^{2+}$. The energies and oscillator strengths of the 80−120 lowest-energy electronic transitions, which involve calculations of the singlet excited-state energies of the complexes, were obtained using time-dependent DFT (TD-DFT) with the same basis sets.

**Synthesis and Characterization.** 7-Amidyl-2,4-dimethyl-1,8-naphthyridine, 7-acetamidyl-2,4-dimethyl-1,8-naphthyridine, and 7-acetamidyl-4-methyl-1,8-naphthyridine-2-aldehyde were synthesized according to the reported procedures.[10] According to modified versions of the reported methods,[11] 7-acetamidyl-4-methyl-2-(1*H*-benzo[*d*]imidazolyl)-1,8-naphthyridine (**A**), 7-acetamidyl-4-methyl-2-(benzo[*d*]oxazolyl)-1,8-naphthyridine (**B**), and 7-acetamidyl-4-methyl-2-(benzo[*d*]thiazolyl)-1,8-naphthyridine (**C**) were synthesized (Scheme 1). The binding modes of **A**−$Ni^{2+}$ and **A**−$Cu^{2+}$ are illustrated in Scheme 2.

**Scheme 1. Synthetic Pathways to Compounds A, B, and C**

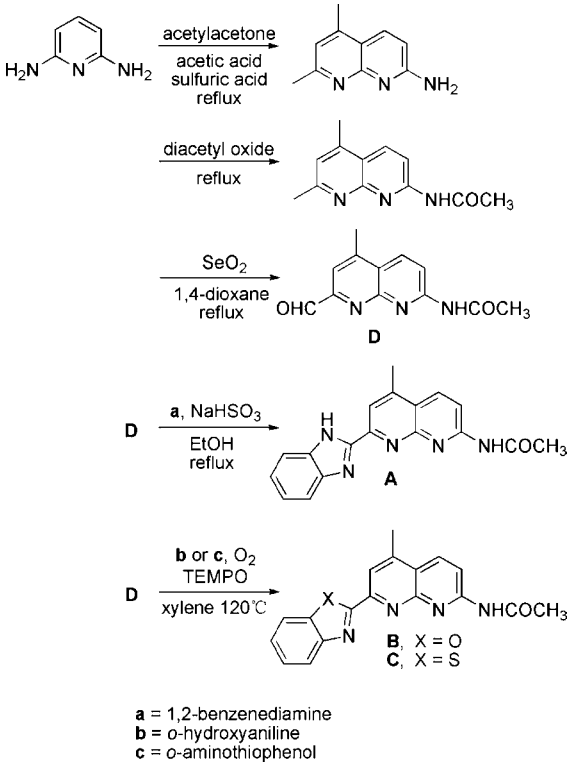


**Scheme 2. Binding Modes of A−$Ni^{2+}$ and A−$Cu^{2+}$ Obtained at the B3LYP/6-31G(d) Level**

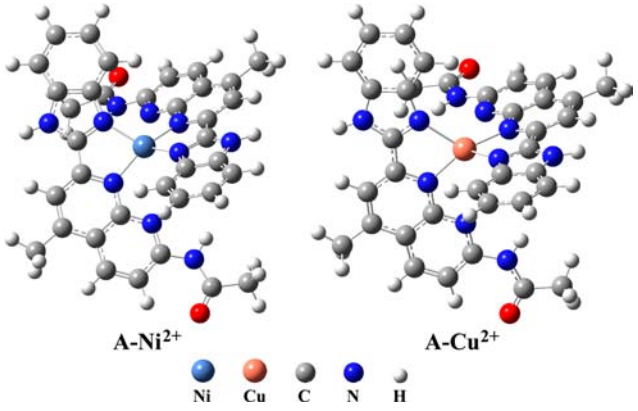


*7-Amidyl-2,4-dimethyl-1,8-naphthyridine.* 7-Amidyl-2,4-dimethyl-1,8-naphthyridine was synthesized and purified from 2,6-diaminopyridine according to a modified version of the literature procedure.[10b,c] Yield: 35%. $^1$H NMR (400 MHz, DMSO-$d_6$, TMS): $\delta_H$ 8.02 (d, 1H, $J$ = 8.8 Hz), 6.88 (s, 1H), 6.76 (d, 1H, $J$ = 8.8 Hz), 6.66 (s, 2H), 2.51 (s, 3H), 2.47 (s, 3H). $^{13}$C NMR (100 MHz, DMSO-$d_6$): $\delta_C$ 160.82, 160.25, 156.86, 1, 145.02, 134.28, 118.95 114.47, 111.97, 25.27, 17.90.

*7-Acetamidyl-2,4-dimethyl-1,8-naphthyridine.* 7-Acetamino-2-methyl-1,8-naphthyridine was synthesized from 7-amidyl-2,4-dimethyl-1,8-naphthyridine according to a modified version of the literature method.[10d,e] Yield: 84%. $^1$H NMR (400 MHz, DMSO-$d_6$, TMS): $\delta_H$ 10.95 (s, 1H) 8.48 (d, 1H, $J$ = 8.8 Hz), 8.30 (d, 1H, $J$ = 8.8 Hz), 7.24 (s, 1H), 2.61 (s, 3H), 2.51 (s, 3H), 2.17 (s, 3H). $^{13}$C NMR (100 MHz, DMSO-$d_6$): $\delta_C$ 170.51, 162.43, 155.03, 154.15, 145.83, 136.31, 122.15, 118.28, 113.72, 25.61, 24.62, 18.01.

*7-Acetamidyl-4-methyl-1,8-naphthyridine-2-aldehyde.* 7-Acetamidyl-2,4-dimethyl-1,8-naphthyridine (2 g, 0.0093 mol) and selenium dioxide (1.3 g, 0.0117 mol) were added to 100 mL of 1,4-dioxane, and the reaction mixture was refluxed for 4 h with stirring under nitrogen. The mixture was filtered while hot, and the crude product was obtained by concentration in vacuum. The final product was obtained by column chromatography over silica gel using 50:1 dichloromethane/ethanol as the eluent (0.86 g, 43% yield). $^1$H NMR (400 MHz, DMSO-$d_6$, TMS): $\delta_H$ 11.19 (s, 1H), 10.05 (s, 1H), 8.63 (d, 1H, $J$ = 9.2 Hz), 8.48 (d, 1H, $J$ = 9.2 Hz), 7.80 (s, 1H), 2.75 (s, 3H), 2.21 (s, 3H). $^{13}$C NMR (100 MHz, DMSO-$d_6$): $\delta_C$ 194.57, 170.85, 155.51, 154.92, 154.48, 148.85, 136.84, 122.70, 117.30, 116.89, 24.70, 18.42.

*7-Acetamidyl-4-methyl-2-(1H-benzo[d]imidazolyl)-1,8-naphthyridine (**A**).* 7-Acetamidyl-4-methyl-1,8-naphthyridine-2-aldehyde (0.2130 g, 0.93 mmol) was added to an ethanol solution of phenylenediamine (0.1807 g, 1.66 mmol) and $NaHSO_3$ (0.2244 g, 2.16 mmol). The above mixture was refluxed for 1.5 h under an argon atmosphere, and the crude product was obtained under vacuum. The final product was obtained by column chromatography (200−300 mesh, 60:1 ethyl acetate/$CH_3OH$) (0.2318 g, 78.6% yield). Decomposition temperature: 230 °C. Characterization of **A**: HRMS (EI) $m/z$: calcd for $C_{18}H_{15}N_5O$ $[M + H]^+$, 318.1277; found, 318.1354. $^1$H NMR (400 MHz, DMSO-$d_6$, TMS): $\delta_H$ 13.15 (s, 1H), 10.76 (s, 1H), 8.57 (d, 1H), 8.36 (d, 1H), 8.31 (s, 1H), 7.67 (d, 2H), 7.26 (m, 2H), 2.75 (s, 3H), 2.22 (s, 3H). $^{13}$C NMR (100 MHz, DMSO-$d_6$): $\delta_C$ 170.69, 154.98, 154.84, 154.73, 151.46, 150.98, 147.73, 136.60, 136.58, 120.74, 119.42, 115.31, 24.78, 18.40.

*7-Acetamidyl-4-methyl-2-(benzo[d]oxazolyl)-1,8-naphthyridine (**B**).* 2-Aminophenol (0.1726 g, 1.58 mmol) and 7-acetamidyl-4-methyl-1,8-naphthyridine-2-aldehyde (0.3496 g, 1.53 mmol) were added to a 25 mL two-neck flask containing xylenes (15 mL; mixture of *m*-, *o*-, and *p*-xylene). After the mixture was allowed to react for 0.5 h at 120 °C, 2,2,6,6-tetramethylpiperidine *N*-oxyl (TEMPO) (4.3 mg) was added. The solution was then stirred for 8 h at 120 °C, and the crude product was obtained under vacuum. The final product was obtained by column chromatography (200−300 mesh, 5:3 ethyl


dx.doi.org/10.1021/ic3018453 | *Inorg. Chem.* 2012, 51, 12444−12449

acetate/light petroleum) (0.3388 g, 71% yield). Mp = 206−208 °C. Characterization of **B**: HRMS (EI) *m*/*z*: calcd for $C_{18}H_{14}N_4O_2$ $[M]^+$, 318.1117; found, 318.1122. $^1$H NMR (400 MHz, $CDCl_3$, TMS): $\delta_H$ 9.32 (s, 1H), 8.63 (d, 1H), 8.43 (d, 1H), 8.32 (s, 1H), 7.86 (d, 1H), 7.70 (d, 1H), 7.44 (m, 2H), 2.81 (s, 3H), 2.37 (s, 3H). $^{13}$C NMR (100 MHz, $CDCl_3$): $\delta_C$ 169.99, 161.32, 154.45, 151.36, 148.39, 147.32, 141.78, 135.63, 126.55, 125.05, 121.46, 120.73, 120.73, 120.58, 116.13, 111.51.

*7-Acetamidyl-4-methyl-2-(benzo[d]thiazolyl)-1,8-naphthyridine (**C**).* The synthetic procedure for **C** was similar to that for **B**, and the yield was 67%. Decomposition temperature: 223 °C. Characterization of **C**: HRMS (EI) *m*/*z*: calcd for $C_{18}H_{14}N_4OS$ $[M]^+$, 334.0888; found, 334.0893. $^1$H NMR (400 MHz, $CDCl_3$, TMS): $\delta_H$ 9.62 (s, 1H), 8.62 (d, 1H), 8.42 (d, 1H), 8.36 (s, 1H), 8.12 (d, 1H), 8.00 (d, 1H), 7.51 (m, 2H), 2.80 (s, 3H), 2.32 (s, 3H). $^{13}$C NMR (100 MHz, $CDCl_3$): $\delta_C$ 169.94, 154.39, 154.33, 154.24, 153.95, 141.14, 136.70, 135.93, 126.41, 126.13, 123.84, 122.20, 121.65, 118.64, 115.62, 25.00, 18.40.

## RESULTS AND DISCUSSION

**Absorption and Fluorescence Properties of Compounds A, B, and C.** The absorption spectra of compounds **A**, **B**, and **C** in aqueous solution [3:1 (v/v) 0.05 M HEPES (pH 7.4)/$C_2H_5OH$] exhibit two bands in the range 330−400 nm (molar extinction coefficients: $\varepsilon_{371} = 2.82 \times 10^4$ $M^{-1}$ $cm^{-1}$, $\varepsilon_{355} = 2.58 \times 10^4$ $M^{-1}$ $cm^{-1}$ for **A**; $\varepsilon_{368} = 5.04 \times 10^4$ $M^{-1}$ $cm^{-1}$, $\varepsilon_{351} = 4.94 \times 10^4$ $M^{-1}$ $cm^{-1}$ for **B**; $\varepsilon_{372} = 3.62 \times 10^4$ $M^{-1}$ $cm^{-1}$, $\varepsilon_{357} = 3.71 \times 10^4$ $M^{-1}$ $cm^{-1}$ for **C**.) (Figure S1 in the Supporting Information). These bands may be assigned to $\pi \rightarrow \pi^*$ electronic transitions. Upon excitation at 370 nm in aqueous solution [3:1 (v/v) 0.05 M HEPES (pH 7.4)/$C_2H_5OH$], the three compounds exhibit very strong fluorescence emission at 433, 399, and 408 nm with $\Phi_{fl}$ = 0.252, 0.877, and 0.511, respectively (Figure S2). The fact that **B** has the highest $\Phi_{fl}$ may be ascribed to its greater planarity and the stronger electron-pushing benzo[*d*]oxazolyl unit.

**Effect of $Ni^{2+}$/$Cu^{2+}$ on the Fluorescence Spectra of A.** Addition of 2 equiv of $NiCl_2$/$CuCl_2$ ($Ni^{2+}$/$Cu^{2+}$, $2.5 \times 10^{-5}$ M) to an aqueous solution of **A** [3:1 (v/v) 0.05 M HEPES (pH 7.4)/$C_2H_5OH$] produced a new absorption band in the 400−500 nm range and a 10 nm red shift of the absorption maximum (Figure 1 left and Figure S3), while the fluorescence

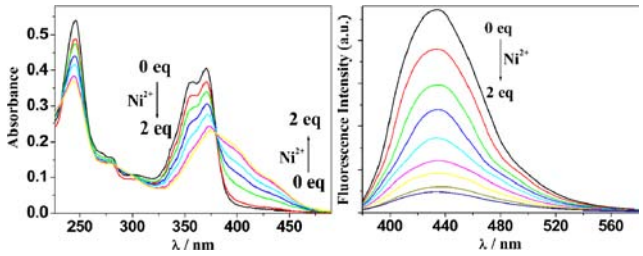


**Figure 1.** (left) Absorption and (right) emission spectral changes for compound **A** in aqueous solution [$1.25 \times 10^{-5}$ M in 3:1 (v/v) 0.05 M HEPES (pH 7.4)/$C_2H_5OH$] upon addition of $NiCl_2$. In (b), the excitation wavelength was 370 nm.

was almost completely quenched ($\Phi_{fl}$ changed from 0.252 to 0.089 and 0.060 with $I/I_0$ = 0.044 and 0.039 for $Ni^{2+}$ and $Cu^{2+}$, respectively) with no change in the emission wavelength (Figure 1 right and Figure S4), indicating efficient $Ni^{2+}$/$Cu^{2+}$-selective on−off behavior.

**Selectivity Study of the Detection of $Ni^{2+}$/$Cu^{2+}$ with A.** Upon the addition of equal amounts of various metal ions ($2.5 \times 10^{-5}$ M), only $Ni^{2+}$ and $Cu^{2+}$ decreased the emission of **A**; under identical conditions, nearly no fluorescence intensity changes were observed in the emission spectrum in the presence of $Mg^{2+}$, $K^+$, $Ca^{2+}$, $Cr^{3+}$, $Mn^{2+}$, $Fe^{3+}$, $Zn^{2+}$, $Cd^{2+}$, $Hg^{2+}$ or $Pb^{2+}$ (light bars in Figure 2 and Figure S5). The left panel of

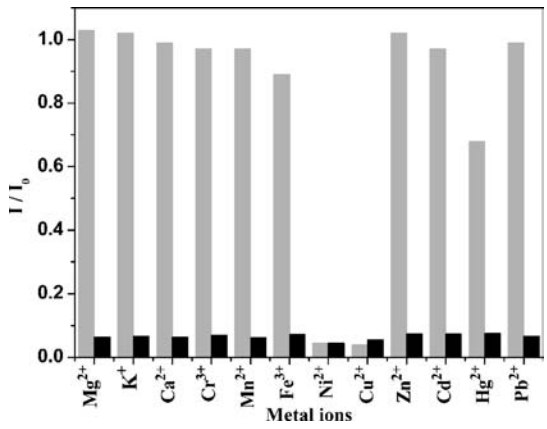


**Figure 2.** Fluorescence responses of **A** [$1.25 \times 10^{-5}$ M in 3:1 (v/v) 0.05 M HEPES (pH 7.4)/$C_2H_5OH$] upon addition of different metal salts (3 equiv of salt ion relative to **A**) (light bars) and fluorescence changes of the mixture of **A** and $Ni^{2+}$ after addition of an excess of the indicated metal ions (12 equiv relative to **A**) (dark bars). The excitation wavelength was 370 nm. For the light gray bars, $I_0$ and $I$ represent the emission intensities at 433 nm in the fluorescence spectra of compound **A** before and after addition of the metal ion to the solution of **A**; for the dark bars, $I_0$ represents the emission intensity at 433 nm in the fluorescence spectrum of compound **A**, and $I$ represents the intensity in the fluorescence spectrum of the mixture of **A** and $Ni^{2+}$ after addition of an excess of the metal ion. The metal salts used were $MgCl_2$, KCl, $CaCl_2$, $CrCl_3$, $MnCl_2$, $FeCl_3$, $NiCl_2$, $CuCl_2$, $ZnCl_2$, $CdCl_2$, $HgCl_2$, and $PbCl_2$.

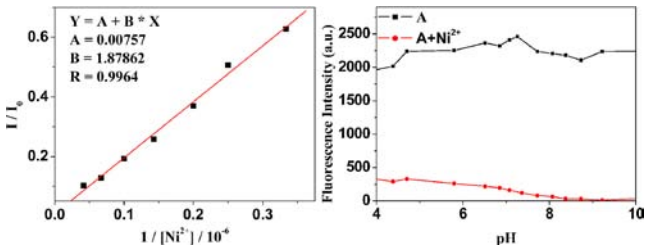


**Figure 3.** (left) Plot of emission intensity of compound **A** at 432 nm (black ■) vs the reciprocal of the concentration of added $Ni^{2+}$. (right) Variation of the fluorescence spectrum of **A** [$1.25 \times 10^{-5}$ M in 3:1 (v/v) 0.05 M HEPES (pH 7.4)/$C_2H_5OH$] with (red ●) and without 1.92 equiv of $Ni^{2+}$ ion (black ■) as a function of pH. The fluorescence intensity was measured at 432 nm.

Figure 3 demonstrates the relationship between the concentration of $Ni^{2+}$ and the emission intensity at the special wavelength. The detection limit of the fluorescence response of the sensor to $Ni^{2+}$ was $6.42 \times 10^{-6}$ M (Figure 3 left). For $Cu^{2+}$, the detection limit was $7.09 \times 10^{-6}$ M (Figure S6), which is satisfactory for the detection of $Cu^{2+}$ in drinking water within U.S. EPA limit (≈20 μM). Job's plots indicated that **A** chelates $Ni^{2+}$/$Cu^{2+}$ with 2:1 stoichiometry, and the binding constants of **A** with $Ni^{2+}$ and $Cu^{2+}$ were calculated to be $2.84 \times 10^9$ and $5.74 \times 10^7$, respectively (Figures S7 and S8). We also found a remarkable selectivity of **A** for $Ni^{2+}$/$Cu^{2+}$ ion over various other


dx.doi.org/10.1021/ic3018453 | Inorg. Chem. 2012, 51, 12444−12449

metal ions, which turned out to be applicable in environmental technology (dark bars in Figure 2 and Figure S5).

**Effect of $Ni^{2+}/Cu^{2+}$ on the Fluorescence Spectra of B and C.** To understand the crucial role of the 1*H*-benzo[*d*]-imidazolyl unit, which behaves as an additional binding site for the $Ni^{2+}/Cu^{2+}$ ions with the aid of the naphthyridine group, we synthesized **B** and **C** bearing benzo[*d*]oxazolyl and benzo[*d*]-thiazolyl units, respectively, on the 7-acetamidyl-4-methyl-1,8-naphthyridine. Subsequently, **B** and **C** were tested for fluorescence changes upon the addition of $Ni^{2+}$ and $Cu^{2+}$ ions as well. As shown in Figure 4 and Figures S9–S12, unlike

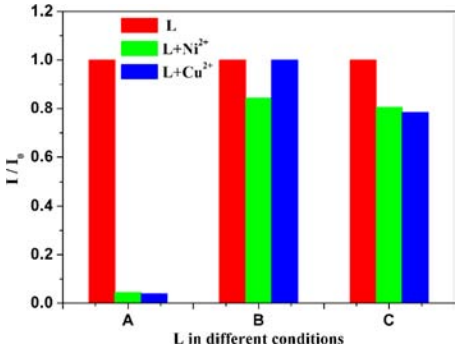


**Figure 4.** Relative fluorescence responses of **A**, **B**, and **C** [$1.25 \times 10^{-5}$ M in 3:1 (v/v) 0.05 M HEPES (pH 7.4)/$C_2H_5OH$] at 433, 400, and 408 nm, respectively, without $Ni^{2+}/Cu^{2+}$ (red bars) and after addition of 3 equiv of $NiCl_2$ (green bars) or $CuCl_2$ (blue bars). Excitation was at 370 nm.

**A**, neither **B** nor **C** showed any distinct absorption or fluorescence spectral changes upon the addition of $Ni^{2+}$ or $Cu^{2+}$ ions. This strongly supports the conclusion that having a nitrogen atom at the 1-position in the substituent at the 2-position of the 7-acetamidyl-4-methyl-1,8-naphthyridine core plays an important role in the $Ni^{2+}/Cu^{2+}$ complexation.

**Computational Study of the Coordinating Abilities of A, B, and C.** To interpret further the influence of the 1*H*-benzo[*d*]imidazolyl unit in the reaction of **A** with metal ions, theoretical calculations were performed on compounds **A**, **B**, and **C**. From Figure 5 and Figures S13–S15, it is obvious that the negative charge density of N4 (−0.412) in the 1*H*-benzo[*d*]imidazolyl unit is higher than those of the benzo[*d*]-oxazolyl (−0.389) and benzo[*d*]thiazolyl (−0.364) units, indicating a stronger coordination ability for N4 in the 1*H*-benzo[*d*]imidazolyl unit in **A** than for the corresponding units in **B** and **C**. Considering the $Ni^{2+}/Cu^{2+}$-induced absorption and emission spectral changes for **A**, **B**, and **C** and the similar negative charge densities of N1, N2, N3 and O1 in **A**, **B**, and **C**, it is easy to conclude that the coordinating atoms should be N3 and N4 (Scheme 2).

**Study of the Fluorescence Decay Behavior.** As is well-known, heavy metal ions tend to quench the luminescence through electron- and/or energy-transfer processes.[8,12] To gain insight into the quenching behavior in the **A**–$Ni^{2+}$ and **A**–$Cu^{2+}$ complexes, we measured picosecond TRF spectra. The fluorescence decay behavior in the presence of $Ni^{2+}/Cu^{2+}$ is shown in Figures S16 to S23, and the double-exponential fit results are summarized in Table 1 and Table S1.

In the absence of $Ni^{2+}/Cu^{2+}$, the fluorescence decayed in a double-exponential manner with time constants of 1.12 and 2.30 ns, indicating that the fluorescence spectra consist of two contributions from free **A**. When $Ni^{2+}$ or $Cu^{2+}$ was titrated into


**A**, X = NH
**B**, X = O
**C**, X = S

| Charge distribution | A | B | C |
|---|---|---|---|
| N1 | -0.630 | -0.630 | -0.630 |
| N2 | -0.460 | -0.461 | -0.460 |
| N3 | -0.384 | -0.381 | -0.384 |
| N4 | -0.412 | -0.389 | -0.364 |
| O1 | -0.598 | -0.597 | -0.598 |

**Figure 5.** (top) Structures of **A**, **B** and **C**, including the labeling of the N atoms. (bottom) Table summarizing the charge densities of selected nitrogen and oxygen atoms.

**Table 1. Fluorescence Decay Time Constants of A in the Presence of $Ni^{2+}$ Ions**

| equiv of $Ni^{2+}$ | $A_1$ | $\tau_1$ (ns) | $A_2$ | $\tau_2$ (ns) | $\chi^2$ |
|---|---|---|---|---|---|
| 0 | 14% | 1.12 | 86% | 2.30 | 1.059 |
| 0.5 | 16% | 0.92 | 84% | 2.20 | 1.010 |
| 1 | 14% | 0.81 | 86% | 2.17 | 0.971 |
| 2 | 13% | 0.79 | 87% | 2.18 | 1.131 |

the solution, the lifetime was almost unchanged under the experimental conditions (Table 1 or Table S1, respectively). From the combined observations of the absorption and emission titration experiments, a static quenching mechanism can be deduced. The fluorophore **A** ligates $Ni^{2+}$ or $Cu^{2+}$, forming a nonfluorescent complex in the ground state. The fluorescence quenching of **A** may result from excited-state energy transfer or charge transfer.

**TD-DFT Calculations of Absorption Properties.** To interpret further the absorption properties of **A** and the **A**–$Ni^{2+}$ and **A**–$Cu^{2+}$ complexes, TD-DFT calculations were performed on this system. In compound **A**, the highest occupied molecular orbital (HOMO) is mainly located on the 1*H*-benzo[*d*]-imidazolyl unit, and the lowest unoccupied molecular orbital (LUMO) is on the naphthyridine group (Figure S24). In **A**–$Ni^{2+}$, the HOMO and LUMO are located on $Ni^{2+}$ and ligand **A**, respectively (Figure S25). In **A**–$Cu^{2+}$, both the HOMO and LUMO are mainly located on **A** (Figure S26). As shown in Table S2, the lowest-energy transition of **A** comes from the HOMO−1 → LUMO and HOMO → LUMO orbital transitions. As shown in Table 2, the lowest-energy transition of **A**–$Ni^{2+}$ comes from the HOMO−4 → LUMO, HOMO−5 → LUMO, HOMO → LUMO+12, HOMO−4 → LUMO+1, and HOMO−10 → LUMO orbital transitions; for **A**–$Cu^{2+}$, the lowest-energy transition comes from the HOMO → LUMO+12 and HOMO−5 → LUMO orbital transitions. The calculated absorption-peak positions are in good agreement with the experimental results (Figures S27–S29), which proves that intramolecular charge-transfer processes occur in the excited states of **A**, **A**–$Ni^{2+}$, and **A**–$Cu^{2+}$.

**TD-DFT Calculations of the Fluorescence Quenching Mechanism.** To elaborate upon the fluorescence quenching


dx.doi.org/10.1021/ic3018453 | *Inorg. Chem.* 2012, 51, 12444–12449

**Table 2. Contributions of Various Orbital Transitions to the Lowest-Energy Transitions in A−$Ni^{2+}$ and A−$Cu^{2+}$**

| | oscillator strength | |
|---|---|---|
| orbital transition | A−$Ni^{2+}$ | A−$Cu^{2+}$ |
| HOMO−10 → LUMO | 0.1313 | |
| HOMO−5 → LUMO | 0.2237 | 0.4151 |
| HOMO−4 → LUMO | 0.1009 | |
| HOMO → LUMO+12 | 0.1436 | 0.4949 |
| HOMO−4 → LUMO+1 | 0.2893 | |

mechanism, we also carried out TD-DFT calculations (Figure 6, Figures S25 and S26, and Table 2). It is noted that the

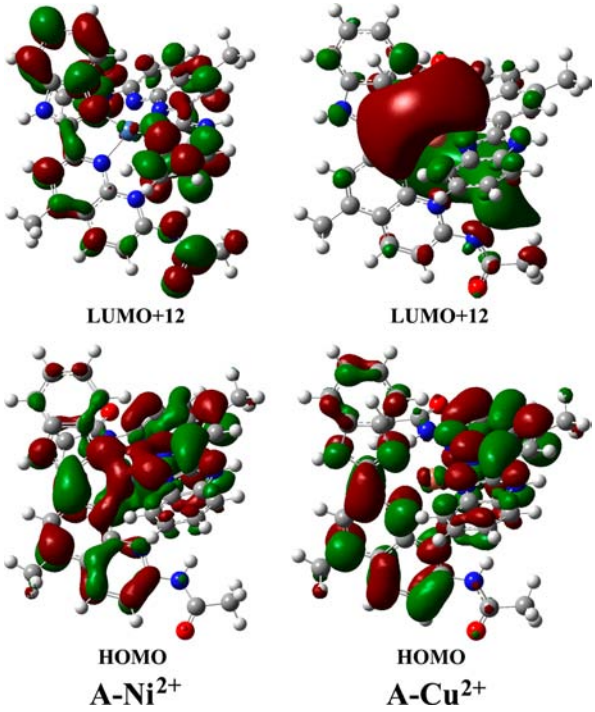


**Figure 6.** Frontier molecular orbitals of A−$Ni^{2+}$ and A−$Cu^{2+}$ relevant to the fluorescence quenching.

fluorescence quenching by $Ni^{2+}$ can be rationalized in terms of the occupancy of the frontier orbitals. The HOMO → LUMO+12 excitation was found to be related to metal-to-ligand charge transfer (MLCT), and its contribution to the lowest-energy excitation was 14.4%. Such excitation corresponds to charge transfer from the excited $Ni^{2+}$ center to the naphthyridine and 1*H*-benzo[*d*]imidazolyl moieties and thus provides a pathway for nonradiative deactivation of the excited state. On the basis of the calculations, the MLCT contribution is ~14.4%. Thus, considering the results of the TRF experiments, energy transfer may also contribute to the nonradiative deactivation of the excited state to a significant extent. As for the fluorescence quenching by $Cu^{2+}$, different calculation results were obtained (Figure 6 and Figure S26). Although the HOMO → LUMO+12 excitations were also found to be relevant for the fluorescence quenching by $Cu^{2+}$, such excitation corresponds to ligand-to-metal charge transfer (LMCT) from the excited naphthyridine and 1*H*-benzo[*d*]-imidazolyl moieties to the $Cu^{2+}$ center and thus provides a pathway for nonradiative deactivation of the excited state. Since the LMCT contribution is ~49.5%, energy transfer may partly contribute to the nonradiative deactivation of the excited state.

**Study of the Reversibility of the Binding of Chemosensor A to $Ni^{2+}$ and $Cu^{2+}$.** To examine the reversibility of the binding of chemosensor **A** to $Ni^{2+}$ and $Cu^{2+}$, an ethanol solution containing 64 equiv of EDA was added to the A−$Ni^{2+}$ and A−$Cu^{2+}$ solutions, respectively. No enhanced emission intensity was observed when EDA was added to the A−$Ni^{2+}$ solution (Figure 7 left). This indicates that EDA is not able to

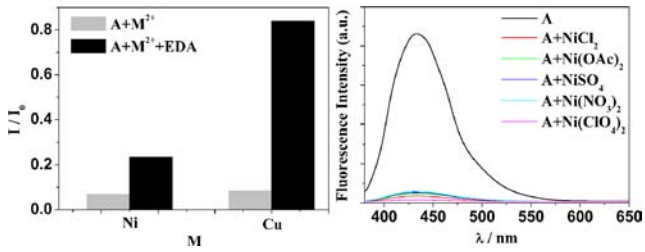


**Figure 7.** (left) Relative fluorescence responses of the complexes A−$Ni^{2+}$ and A−$Cu^{2+}$ [$1.25 \times 10^{-5}$ M in 3:1 (v/v) 0.05 M HEPES (pH 7.4)/$C_2H_5OH$] before (light bars) and after (dark bars) the addition of EDA. Excitation was at 370 nm, and emission was monitored at 432 nm. (right) Fluorescence emission spectra of **A** [$1.25 \times 10^{-5}$ M in 3:1 (v/v) 0.05 M HEPES (pH 7.4)/$C_2H_5OH$] upon addition of different nickel salts ($2.4 \times 10^{-5}$ M) with excitation at 370 nm.

remove $Ni^{2+}$ ions from the A−$Ni^{2+}$ complex and hence cannot restore the emission of **A**. However, when EDA was added to the A−$Cu^{2+}$ solution, fluorescence signals identical to those of **A** were restored (Figure 7 left and Figure S30), demonstrating that $Cu^{2+}$ is removed from the A−$Cu^{2+}$ complex by EDA. That is, the binding of **A** and $Cu^{2+}$ is really chemically reversible. In other words, EDA showed high selectivity toward the in situ-prepared $Cu^{2+}$ complex over the $Ni^{2+}$ complex, which can be applied to distinguish $Ni^{2+}$ and $Cu^{2+}$.

**Counterion Effect on the $Ni^{2+}$/$Cu^{2+}$-Selective Properties of A.** Experiments to explore the counterion effect on the $Ni^{2+}$/$Cu^{2+}$-selective properties of **A** were also performed (Figure 7 right and Figure S31). Acetate, sulfate, nitrate, and perchlorate counteranions had similar influence as chloride when it comes to $Ni^{2+}$ and $Cu^{2+}$ salts, demonstrating that the anions do not coordinate the metal ions while compound **A** reacts with $Ni^{2+}$ or $Cu^{2+}$. This indicates that compound **A** as a fluorescent sensor has a much wider application range in sensing $Ni^{2+}$ and $Cu^{2+}$ ions.

**pH Range of Application of A toward $Ni^{2+}$ and $Cu^{2+}$.** For both environmental and biological applications of the fluorescent sensor, it would be much better if the sensing works over a wide range of pH. The right panel of Figure 3 shows that in aqueous solution the suitable pH range for $Ni^{2+}$ determination is 4−10, where the fluorescence on−off behavior can be operated by $Ni^{2+}$ binding. Consequently, our present $Ni^{2+}$-selective receptor would be an ideal fluorometric chemosensor for monitoring $Ni^{2+}$. Similar results were obtained for $Cu^{2+}$ (Figure S32).

**In Situ Imaging and Intracellular $Ni^{2+}$/$Cu^{2+}$ Response.** It is essential for biosensing molecules to monitor guest species selectively in living cells for biological applications.[13] The $Ni^{2+}$/$Cu^{2+}$ sensitivity of **A** was examined in living cells by using confocal microscopy. Human lung adenocarcinoma epithelial cells (A549) were selected for our experiments. Fluorescence images were recorded with excitation at 408 nm by a diode


dx.doi.org/10.1021/ic3018453 | *Inorg. Chem.* 2012, 51, 12444−12449

laser, spinhole aperture, 100% gain of detector, and an oil objective with 60× magnification and 1.40 NA. The qualitative in vitro results are shown in Figure 8 and Figure S33. After

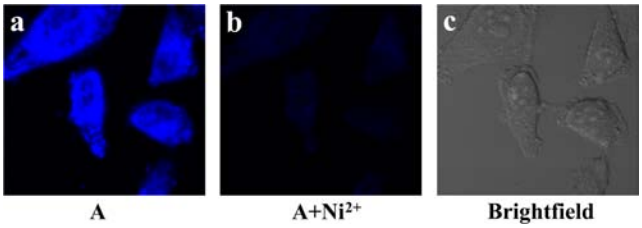


**Figure 8.** In situ imaging and intracellular $Ni^{2+}$ response of **A**-labeled living cells at 37 °C. (a) A549 cells incubated with 0.01 μmol of compound **A** and 1 mL of PBS for 30 min at 37 °C. (b) A549 cells from (a) 10 min after treatment with 0.03 μmol of $Ni^{2+}$ in aqueous solution. (c) Bright-field image of living A549 cells.

A549 cells were incubated with 0.01 μmol of **A** and 1 mL of phosphate-buffered saline (PBS) for 30 min at 37 °C, very strong fluorescence was imaged (Figure 8a and Figure S33a). These **A**-containing A549 cells were then incubated with 0.03 μmol of $Ni^{2+}/Cu^{2+}$ for another 10 min. No obvious fluorescence was imaged (Figure 8b and Figure S33b) because of the quenching of the emission of **A** by $Ni^{2+}/Cu^{2+}$.

## CONCLUSIONS

A highly fluorescent 1,8-naphthyridine-derived chemosensor with high sensitivity and selectivity toward $Ni^{2+}/Cu^{2+}$ over other cations both in aqueous solution over a wide pH range (4−10) and in a cellular environment was developed. Counteranions such as acetate, sulfate, nitrate, and perchlorate have no influence on the detection of such metal ions. EDA showed high selectivity toward the in situ-prepared $Cu^{2+}$ complex over the $Ni^{2+}$ complex, which can be applied to distinguish $Ni^{2+}$ and $Cu^{2+}$. The fluorescence on−off mechanism was revealed to be mediated by intramolecular charge transfer, as confirmed by picosecond time-resolved fluorescence spectroscopy and time-dependent density functional theory calculations.

## ASSOCIATED CONTENT

### Supporting Information

Absorbance and fluorescence spectra of **A**, **B**, and **C** in their metal-free and metal-bound forms, Job's plot, TRF spectra, and calculation details for **A** in the presence of $Ni^{2+}/Cu^{2+}$. This material is available free of charge via the Internet at http://pubs.acs.org.

## AUTHOR INFORMATION

### Corresponding Author

*E-mail: lizx@zzu.edu.cn (Z.L.), yumm@zzu.edu.cn (M.Y.), zhanghongyan@mail.ipc.ac.cn (H.Z.). Tel: +86-371-67781205. Fax: +86-731-67781205.

### Notes

The authors declare no competing financial interest.

## ACKNOWLEDGMENTS

This work was supported by the National Natural Science Foundation of China (50903075, 60978034, and 50873093). We are grateful to Professor Chenjie Fang at Capital Medical University for her great help with our manuscript.

## REFERENCES

(1) (a) Valeur, B.; Leray, I. *Coord. Chem. Rev.* **2000**, *205*, 3−40. (b) Pawley, J. B. *Handbook of Biological Confocal Microscopy*; Plenum Press: New York, 1995. (c) Lichtman, J. W.; Conchello, J. A. *Nat. Methods* **2005**, *2*, 910−919.

(2) (a) Xu, Z.; Yoon, J.; Spring, D. R. *Chem. Soc. Rev.* **2010**, *39*, 1996−2006. (b) Kikuchi, K. *Chem. Soc. Rev.* **2010**, *39*, 2048−2053. (c) Wu, J.; Liu, W.; Ge, J.; Zhang, H.; Wang, P. *Chem. Soc. Rev.* **2011**, *40*, 3483−3495. (d) Quang, D. T.; Kim, J. S. *Chem. Rev.* **2010**, *110*, 6280−6301.

(3) *Nickel and Its Surprising Impact in Nature*; Sigel, A., Sigel, H., Sigel, R. K. O., Eds.; Metal Ions in Life Sciences, Vol. *2*; Wiley: Chichester, U.K., 2007.

(4) (a) Banerjee, A.; Sahana, A.; Guha, S.; Lohar, S.; Hauli, I.; Mukhopadhyay, S. K.; Matalobos, J. S.; Das, D. *Inorg. Chem.* **2012**, *51*, 5699−5704. (b) Li, G.; Fang, H.; Cai, Y.; Zhou, Z.; Thallapally, P. K.; Tian, J. *Inorg. Chem.* **2010**, *49*, 7241−7243. (c) Dodani, S. C.; He, Q.; Chang, C. J. *J. Am. Chem. Soc.* **2009**, *131*, 18020−18021.

(5) (a) Rurack, K. *Spectrochim. Acta, Part A* **2001**, *57*, 2161−2195. (b) Kramer, R. *Angew. Chem., Int. Ed.* **1998**, *37*, 772−773. (c) Muthaup, G.; Schlicksupp, A.; Hess, L.; Beher, D.; Ruppert, T.; Masters, C. L.; Beyreuther, K. *Science* **1996**, *271*, 1406−1409. (d) Løvstad, R. A. *BioMetals* **2004**, *17*, 111−113. (e) Barnham, K. J.; Masters, C. L.; Bush, A. I. *Nat. Rev. Drug Discovery* **2004**, *3*, 205−214.

(6) Georgopoulos, P. G.; Roy, A.; Yonone-Lioy, M. J.; Opiekun, R. E.; Lioy, P. J. *J. Toxicol. Environ. Health, Part B* **2001**, *4*, 341−394.

(7) (a) Li, Z.; Zhang, L.; Wang, L.; Guo, Y.; Cai, L.; Yu, M.; Wei, L. *Chem. Commun.* **2011**, *47*, 5798−5800. (b) Lau, Y. H.; Price, J. R.; Todd, M. H.; Rutledge, P. J. *Chem.—Eur. J.* **2011**, *17*, 2850−2858. (c) Zhao, Y.; Zhang, X.; Han, Z.; Qiao, L.; Li, C.; Jian, L.; Shen, G.; Yu, R. *Anal. Chem.* **2009**, *81*, 7022−7029. (d) Domaille, D. W.; Zeng, L.; Chang, C. J. *J. Am. Chem. Soc.* **2010**, *132*, 1194−1195. (e) Kumar, M.; Dhir, A.; Bhalla, V. *Org. Lett.* **2009**, *11*, 2567−2569. (f) Jung, H. S.; Park, M.; Han, D. Y.; Kim, E.; Lee, C.; Ham, S.; Kim, J. S. *Org. Lett.* **2009**, *11*, 3378−3381. (g) Kim, H. J.; Hong, J.; Hong, A.; Ham, S.; Lee, J. H.; Kim, J. S. *Org. Lett.* **2008**, *10*, 1963−1966. (h) Zhou, Y.; Wang, F.; Kim, Y.; Kim, S.; Yoon, J. *Org. Lett.* **2009**, *11*, 4442−4445. (i) Yu, M.; Shi, M.; Chen, Z.; Li, F.; Li, X.; Gao, Y.; Xu, J.; Yang, H.; Zhou, Z.; Yi, T.; Huang, C. *Chem.—Eur. J.* **2008**, *14*, 6892−6900. (j) Zhao, Q.; Li, F.; Huang, C. *Chem. Soc. Rev.* **2010**, *39*, 3007−3030. (k) Yu, M.; Li, Z.; Wei, L.; Wei, D.; Tang, M. *Org. Lett.* **2008**, *10*, 5115−5118.

(8) Jung, H. S.; Kwon, P. S.; Lee, J. W.; Kim, J. I.; Hong, C. S.; Kim, J. W.; Yan, S.; Lee, J. Y.; Lee, J. H.; Joo, T.; Kim, J. S. *J. Am. Chem. Soc.* **2009**, *131*, 2008−2012.

(9) Demas, J. N.; Grosby, G. A. *J. Phys. Chem.* **1971**, *75*, 991−1024.

(10) (a) Li, Z.; Yu, M.; Zhang, L.; Yu, M.; Liu, J.; Wei, L.; Zhang, H. *Chem. Commun.* **2010**, *46*, 7169−7171. (b) Henry, R. A.; Hammond, P. R. *J. Heterocycl. Chem.* **1977**, *14*, 1109−1114. (c) Fan, N. Y. *Organic Synthesis*; Beijing University of Technology Press: Beijing, China, 1995; p 183. (d) Kelly, T. R.; Zhao, C.; Bridger, G. J. *J. Am. Chem. Soc.* **1989**, *111*, 3744−3745. (e) Kelly, T. R.; Bridger, G. J.; Zhao, C. *J. Am. Chem. Soc.* **1990**, *112*, 8024−8034. (f) Li, Z.; Fu, W.; Yu, M.; Zhao, X.; Chen, Y. *Dyes Pigm.* **2007**, *75*, 516−520.

(11) (a) Chen, Y. X.; Qian, L. F.; Zhang, W.; Han, B. *Angew. Chem., Int. Ed.* **2008**, *47*, 9330−9333. (b) Liu, Z.; Zhang, C.; Li, Y.; Wu, Z.; Qian, F.; Yang, X.; He, W.; Gao, X.; Guo, Z. *Org. Lett.* **2009**, *11*, 795−798.

(12) (a) Kavallieratos, K.; Rosenberg, J. M.; Chen, W. Z.; Ren, T. *J. Am. Chem. Soc.* **2005**, *127*, 6514−6515. (b) Zheng, Y.; Orbulescu, J.; Ji, X.; Andreopoulos, F. M.; Pham, S. M.; Leblanc, R. M. *J. Am. Chem. Soc.* **2003**, *125*, 2680−2686.

(13) (a) Chang, M. C. Y.; Pralle, A.; Isacoff, E. Y.; Chang, C. J. *J. Am. Chem. Soc.* **2004**, *126*, 15392−15393. (b) Peng, X.; Du, J.; Fan, J.; Wang, J.; Wu, Y.; Zhao, J.; Sun, S.; Xu, T. *J. Am. Chem. Soc.* **2007**, *129*, 1500−1501.